EPJ Web of Conferences **380**, 02010 (2026) https://doi.org/10.1051/epjconf/202638002010
ICISCT'25

ADRC Strategy-Based Control for Grid-Connected PV System using a Single-Phase Modular Multilevel Converter

Amine El Boudali[1,*], *Abdelmajid* Abouloifa[1], *Ouijdane* Arich[1], and *Nouhaila* Hourri[1]

[1]ESE Lab., ENSEM Casablanca. Hassan II University of Casablanca. BP 8118 Casablanca, Morocco

Abstract. This paper deals with the control design of a single-phase Modular Multilevel Converter (MMC) interfaced with a photovoltaic (PV) system. The proposed strategy aims to simultaneously achieve two main objectives: i) power factor correction (PFC) on the grid side to improve power quality, and ii) regulation of the PV voltage to ensure precise maximum power point tracking (MPPT). To fulfill these objectives, a cascaded two-loop control structure is developed, in the outer loop, a filtered proportional–integral (FPI) controller is employed, while an Active Disturbance Rejection Control (ADRC) technique is adopted in the inner loop to enhance dynamic performance and disturbance rejection capability. In addition, a comparative analysis with conventional control approaches is carried out to highlight the effectiveness and robustness of the proposed method. The performance of the suggested controller is verified using MATLAB/Simulink simulation, and the obtained results demonstrate fast dynamic response, accurate tracking performance, and stable operation under different operating conditions.

1 Introduction

The increasing global requirement for cleaner, renewable energy has accelerated the development and integration of Renewable Energy Sources (RES), such as solar and wind, at a rapid pace. RES has numerous positive economic and environmental effects, but with them come many challenges to grid stability [1], power quality, and conversion efficiency. To counteract them, high-performance power electronic converters have a critical role in providing seamless RES integration into modern power networks [2, 3].

Among the many converter topologies, one that stands out for its high performance in high-power applications is the Modular Multilevel Converter (MMC) [4]. It is especially well-suited for High Voltage Direct Current (HVDC) transmission [5], Flexible AC Transmission Systems (FACTS) [6], and integrating renewable energy sources into the grid because of its high efficiency, adaptability, outstanding harmonic performance, and high degree of scalability.

Furthermore, this kind of MMC technology is currently being investigated more and more for AC / DC Hybrid Microgrid (HMG) [7], which combines the benefits of both AC and DC networks to improve system efficiency, flexibility, and dependability. MMC serves as a crucial interface between the AC and DC subsystems in these microgrids, facilitating voltage

*e-mail: amine.elboudali-etu@etu.univh2c.ma

regulation, bidirectional power flow, and enhanced power quality. Therefore, MMC is essential for the creation of robust, effective, and future energy distribution networks [7].

In [8–10], several linear and non-linear controllers for MMC have been put forth and used; all controllers share a common goal: to stabilize the system and maintain dynamic stability. MMC control using a Proportional-Integral (PI) controller is widely used [8], but it has major drawbacks due to the complexity and non-linearities of the system. It does not efficiently manage circulating currents, is sensitive to parametric variations, and has low robustness against harmonics. In addition, its limited bandwidth reduces the responsiveness to disturbances and transients. There are also other control methods for MMC, namely Sliding Mode Control (SMC), which allows us to handle the nonlinearities of the system, offers a fast convergence to the reference, and maintains a stable performance even in the presence of disturbances, such as circulating currents and load variations. However, the implementation of SMC can be complex due to the need for an adequate design of the sliding surface [9].

In the past few years, Active Disturbance Rejection Control (ADRC), originally proposed by Han in 1998, has attracted considerable attention in various areas of control engineering as a promising alternative to traditional PID regulators and model-based control approaches [11]. To simplify the implementation of the nonlinear ADRC structure, the study in [12] introduced a Linear Active Disturbance Rejection Control (LADRC) scheme, where nonlinear functions were replaced by linear gains. Unlike many conventional control methods, ADRC does not rely on an accurate mathematical model of the system, which makes its implementation simpler and reduces the complexity associated with parameter tuning [13]. In addition, the controller order can be selected flexibly according to the application requirements, allowing ADRC to be adopted in a wide range of systems. Owing to these characteristics, ADRC offers several advantages such as fast dynamic response, high tracking precision, strong disturbance rejection capability, and reliable system stability.

The present paper proposes an approach to improving the performance of a grid-connected PV–MMC system through the implementation of a first-order ADRC. One of the main advantages of the proposed topology lies in its ability to achieve effective compensation performance while employing a reduced number of semiconductor devices. The proposed control strategy is organized into two cascaded loops, namely an inner loop and an outer loop. The inner loop is designed based on the ADRC technique to regulate the grid current and circulating current, providing strong robustness against disturbances, parameter uncertainties, and external perturbations, while ensuring fast dynamic response and outstanding steady-state behavior. A nonlinear PI-based control loop with a filtering method controls the DC-link voltage to manage the voltage of the PV array and ensure its convergence toward the desired reference value. In addition, Maximum Power Point Tracking (MPPT) is achieved using the Perturb and Observe (P&O) algorithm due to its simplicity and adaptability under rapidly varying atmospheric conditions. Furthermore, a comparative study with conventional control methods, including PI and Proportional Resonant (PR) controllers, is carried out to evaluate the effectiveness of the proposed ADRC-based approach.

This work's main contributions are summarized as follows:

- Application of the ADRC technique in the inner control loop for simultaneous regulation of the grid current and circulating current in a single-phase PV-connected MMC, leading to enhanced robustness and disturbance rejection capability.
- Design of an outer-loop control based on a filtered nonlinear PI regulator combined with the MPPT P&O algorithm to ensure accurate PV voltage regulation, efficient maximum power extraction, and power factor correction (PFC).
- Comparative performance analysis with conventional PI and PR controllers, demonstrating that the proposed strategy provides faster dynamic response, improved disturbance sup-

pression, accurate reference tracking, and unity power factor operation under irradiance variations.

The remainder of this paper is organized as follows. Section 2 presents the mathematical modeling and dynamic analysis of the PV–MMC system. Section 3 describes the proposed ADRC-based control design. Simulation results and performance discussions are provided in Section 4. Lastly, the main findings of this work are provided in Section 5.

2 Dynamics & Mathematical Model

The system under study is a PV system that interacts with the grid through a single-phase MMC, as shown in figure 1. It is composed of: i) a PV array connected to the electrical power grid via an MMC; ii) a single-phase MMC that includes a series of Half-Bridge Submodules (HF-SM) in upper and lower arms.

The HF-SM, as shown in figure 1, consists of a capacitor with voltage v_c connected across two complementary switches, S_1 and S_2, each of which has an antiparallel diode. The current in this circuit can flow in both positive and negative directions [10].

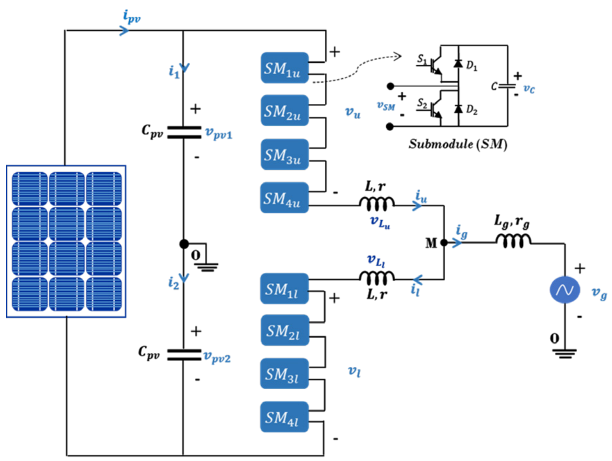

Figure 1. Diagrammatic representation of the MMC supplied by a PV generator.

The state-space mathematical representation of the PV-MMC system is derived from the equivalent circuit illustrated in Figure 1. In this configuration, the variables v_{pv1} and v_{pv2} denote the output voltages of the photovoltaic sources, while i_{pv1} and i_{pv2} correspond to their generated currents. The quantities v_u, i_u, v_l, and i_l represent the capacitor voltages and arm currents associated with the upper and lower branches, respectively. Moreover, i_g and v_g indicate the grid current and grid voltage, where the latter can be expressed as follows:

$$v_g(t) = V_g sin(\omega_g t) \tag{1}$$

In this expression, the symbol V_g represents the magnitude of the grid voltage, while the symbol ω_g represents the angular frequency of the grid voltage. The grid current can be expressed as:

$$i_g(t) = i_u(t) - i_l(t) \tag{2}$$

The currents of the MMC converter are defined as:

$$i_u(t) = i_c(t) + \tfrac{1}{2} i_g(t) \tag{3}$$
$$i_l(t) = i_c(t) - \tfrac{1}{2} i_g(t) \tag{4}$$
$$i_c(t) = \tfrac{1}{2} \left(i_u(t) + i_l(t)\right) \tag{5}$$

By applying Kirchhoff's rules, the mathematical model is as follows:

$$L_1 \frac{di_g}{dt} = -r_1 i_g + \frac{1}{2}\left(v_{pv1} - v_{pv2}\right) - v_g + \frac{1}{2}\left(v_l - v_u\right) \tag{6.a}$$
$$L_2 \frac{di_u}{dt} = -r_2 i_u + \frac{1}{2}\left(\delta v_{pv1} + v_{pv2}\right) - Z i_g + \frac{L}{2L_g} v_g - \frac{1}{2}\left(\delta v_u - v_l\right) \tag{6.b}$$
$$L_2 \frac{di_l}{dt} = -r_2 i_l + \frac{1}{2}\left(v_{pv1} + \delta v_{pv2}\right) + Z i_g + \frac{L}{2L_g} v_g - \frac{1}{2}\left(\delta v_l - v_u\right) \tag{6.c}$$
$$C_{pv} \frac{di_{pv}}{dt} = i_{pv} - i_u \tag{6.d}$$
$$C_{pv} \frac{di_{pv}}{dt} = i_{pv} - i_l \tag{6.e}$$

where

$$L_1 = \left(L_g + \tfrac{L}{2}\right) \qquad L_2 = \left(1 + \tfrac{L}{2L_g}\right) L$$
$$r_1 = \left(r_g + \tfrac{r}{2}\right) \qquad r_2 = \left(1 + \tfrac{r}{2r_g}\right)$$
$$\delta = \left(1 + \tfrac{L}{L_g}\right) \qquad Z = -\tfrac{r}{2} + \tfrac{L}{2L_g} r_g$$

and the upper and lower arm voltage represented as follows:

$$v_u = \sum_{i=1}^{\frac{n}{2}} \tfrac{1+\mu_i}{2} v_{ci} \tag{7.a}$$
$$v_l = \sum_{i=\frac{n}{2}+1}^{n} \tfrac{1-\mu_i}{2} v_{ci} \tag{7.b}$$

It should be noted that there is a relationship between the circulation current i_c and the arm currents i_u and i_l, in (5). The model will be reduced to the fourth order as follows:

$$L_1 \frac{di_g}{dt} = -r_1 i_g + \frac{1}{2} v_{pv,d} - v_g + \frac{1}{2}\left(v_l - v_u\right) \tag{8.a}$$
$$L_2 \frac{di_c}{dt} = -r_2 i_c + \frac{\delta + 1}{4} v_{pv,s} + \frac{L}{2L_g} v_g - \frac{\delta}{4}\left(v_u + v_l\right) - \frac{1}{4}\left(v_u + v_l\right) \tag{8.b}$$
$$C_{pv} \frac{dv_{pv_1}}{dt} = i_{pv} - i_u \tag{8.c}$$
$$C_{pv} \frac{dv_{pv_2}}{dt} = i_{pv} - i_l \tag{8.d}$$

where $v_{pv,s}$ and $v_{pv,d}$ denote the sum and differential components of the PV voltages, defined as $v_{pv,s} = v_{pv1} + v_{pv2}$ and $v_{pv,d} = v_{pv1} - v_{pv2}$, respectively.

The inverter switching function μ_i is defined by:

$$\mu_i = \begin{cases} +1 & \text{if } S_1 \text{ is ON, } S_2 \text{ is OFF,} \\ -1 & \text{if } S_1 \text{ is OFF, } S_2 \text{ is ON.} \end{cases}$$

To achieve the objectives of this study, the variable μ_i must be controlled. The IGBTs are intended to be regulated through the use of a Pulse Width Modulation (PWM) block, and by comparing the modulating reference waveform via a triangular carrier signal that is symmetrical, the PWM blocks produce signals. The creation of pulses for the MMC's upper and lower arms is made easier by this comparative procedure.

3 System Controller Design

The design of a non-linear cascaded controller is the goal of this section. The inner regulator on the grid side is made to guarantee the unity power factor while also ensuring regulation of the circulating current in the MMC. The external regulator is made to ensure that the voltage across the photovoltaic panel is strictly regulated by MPPT. Figure 2 depicts the framework utilized for the fully regulated system.

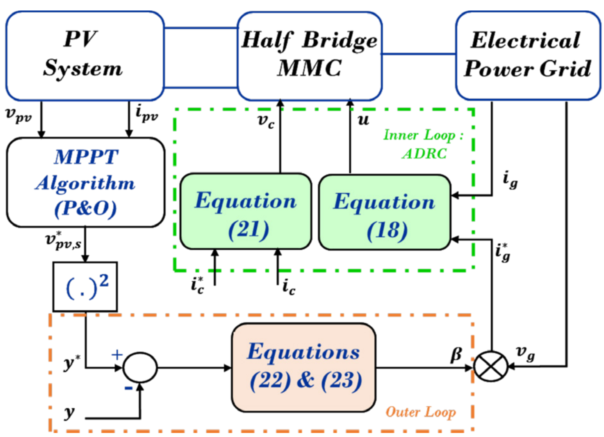

Figure 2. Controller structure

3.1 The LADRC Concept

Active Disturbance Rejection Control, introduced by Han [11, 14], is a robust control technique that compensates for modeling uncertainties and external disturbances in real time. ADRC extends the system model with an Extended State Observer (ESO) to observe unknown dynamics and disturbances. The estimate provided by the extended state observer is used to decouple the system from disturbances, allowing it to be treated as a simplified model for control design [11]. The linear ADRC concept is presented using a first-order system with input u and output y:

$$\frac{dy}{dt} = f(x, d, t) + b_0 u(t) \tag{9}$$

In this expression, f denotes the entire disturbance, d represents the external disturbance, and b is a known system parameter.

The core concept of ADRC involves the use of an ESO to estimate $\hat{f}(t)$. This estimate enables the controller to effectively counteract the influence of $f(t)$ on the system.

$$\begin{cases} \dot{x}_1 = x_2 + b_0 u \\ \dot{x}_2 = \dot{f} \\ y = x_1 \end{cases} \tag{10}$$

In the form of a matrix:

$$\begin{cases} \dot{x} = Ax + Bu + D\dot{f} \\ y = Cx \end{cases} \tag{11}$$

where :

$$A = \begin{pmatrix} 0 & 1 \\ 0 & 0 \end{pmatrix}, \quad B = \begin{pmatrix} b_0 \\ 0 \end{pmatrix}, \quad C = \begin{pmatrix} 1 & 0 \end{pmatrix}, \quad D = \begin{pmatrix} 0 & 1 \end{pmatrix}$$

The entire disturbance can only be calculated via the ESO because it cannot be measured directly, which is constructed based on the system's input and output [14].

The ESO's equations are as follows:

$$\begin{cases} \dot{Z} = AZ + Bu + D(y - \hat{y}) \\ \hat{y} = CZ \end{cases} \tag{12}$$

where :

$$Z = \begin{bmatrix} z_1 & z_2 \end{bmatrix}^T, \quad D = \begin{bmatrix} \beta_1 & \beta_2 \end{bmatrix}^T$$

In this context, D denotes the observer gain. The variables z_1 and z_2 are the estimates of y and f, respectively, the latter being the ESO outputs,

Consequently, the extended state observer's system of equations is provided as follows:

$$\begin{cases} \dot{\hat{z}}_1 = \hat{z}_2 + \beta_1(y - \hat{z}_1) + b_0 u \\ \dot{\hat{z}}_2 = \beta_2(y - \hat{z}_1) \end{cases} \tag{13}$$

The bandwidth parameterization technique is used to select the observer gains under the requirement that all of the matrix's eigenvalues $(A - DC)$ be set to $(-\omega_0)$ [13].

$$\begin{cases} \beta_1 = 2\omega_0 \\ \beta_2 = \omega_0^2 \end{cases} \tag{14}$$

In this expression, ω_0 is the observer's ESO's bandwidth, which is determined by the pole placement method.

The control law for first-order ADRC is expressed as follows.

$$u_0(t) = k_p\,(r(t) - \hat{z}_1(t)) \tag{15.a}$$

$$u(t) = \frac{u_0(t) - \hat{z}_2(t)}{b_0} \tag{15.b}$$

In this formulation, k_p denotes the linear ADRC gain parameter, whereas $r(t)$ stands for the reference input signal, yielding the following relationship:

$$\begin{cases} k_p = \omega_c \\ \omega_0 = 3 \sim 7\omega_c \end{cases} \tag{16}$$

the parameter ω_c denotes the controller bandwidth.

Thus, it can be concluded that the linear ADRC is capable of being controlled by a single parameter k_p. In the meantime, this control strategy's simplification greatly facilitates its use in the industrial sector. The block diagram of the linear ADRC applied to a first-order system is shown in figure 3.

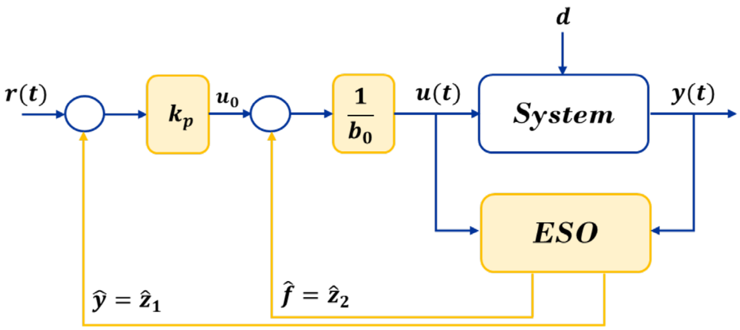

Figure 3. LADRC schematic representation

3.2 LADRC's Control of PV-MMC: Inner Loop

3.2.1 Grid Current Regulator

The PFC aim requires that the power network's input current i_g follow a sinusoidal reference signal $i_g^* = \beta v_g$. The current control loop will now be designed using the LADRC control.

According to (8.a), the following expression for the current of the grid is obtained:

$$\frac{di_g}{dt} = -\frac{r_1}{L_1} i_g + \frac{v_{pv,d}}{2L_1} - \frac{v_g}{L_1} - \frac{nv_c}{4L_1} u \tag{17}$$

It is formulated as:

$$\frac{dx_g}{dt} = f_g\left(x_g, t\right) + b_g u(t) \tag{18}$$

where

$$\begin{cases} i_g = x_g \\ f_g\left(x_g, t\right) = -\frac{r_1}{L_1} x_g + \frac{v_{pv,d}}{2L_1} - \frac{1}{L_1} v_g \\ b_g = -\frac{nv_c}{4L_1} \end{cases}$$

The first-order LADRC control law of the PV-MMC system is as follows:

$$u_0(t) = k_{pi}\left(x_g^*(t) - \hat{z}_1(t)\right) \tag{19.a}$$

$$u(t) = \frac{u_0(t) - \hat{z}_2(t)}{b_g} \tag{19.b}$$

The total disturbance impacting the current of the grid x_g is represented by the variable f_g. The variable u indicates the current loop control input, and the system's known parameters are represented by b_g. The ADRC controllers' k_{pi}, β_1, and β_2 parameters are carefully selected, which will ensure that the current of the grid x_g follows its reference x_g^*.

3.2.2 Circulating Current Regulator

The objective of this subsection is to control the system's circulating current i_c to follow its intended value i_c^* using the ADRC technique. To achieve this, we base our approach on (8.b):

$$\frac{di_c}{dt} = -\frac{r_2}{L_2} i_c + \frac{v_{pv,s}}{4L_2}(\delta + 1) - \frac{L}{2L_g L_2} v_g - \frac{1}{L_2}(1 + \delta) v_c \tag{20}$$

It can be written as follows:

$$\frac{dx_c}{dt} = f_c\left(x_c, t\right) + b_c v_c(t) \tag{21}$$

where

$$\begin{cases} i_c = x_c \\ f_c\left(x_c, t\right) = -\dfrac{r_2}{L_2} x_c + \dfrac{v_{pv,s}}{4L_2}(\delta + 1) - \dfrac{L}{2L_g L_2} v_g \\ b_c = -\dfrac{1}{L_2}(1 + \delta) \end{cases}$$

Finally, the first-order LADRC control law of the circulating current is:

$$v_0(t) = k_{pi}\left(x_c^*(t) - \hat{z}_{1c}(t)\right) \tag{22.a}$$

$$v_c(t) = \frac{v_0(t) - \hat{z}_{2c}(t)}{b_c} \tag{22.b}$$

3.3 Outer Loop

3.3.1 PV Generator Reference

The MPPT "P&O" algorithm is employed to achieve the highest energy conversion efficiency, as it is simple to use and requires less computing time. The method necessitates two input signals, $v_{pv,s} = v_{pv1} + v_{pv2}$ and $i_{pv} = i_{pv1} + i_{pv2}$, to track the voltage $v_{pv,s}^*$ that the photovoltaic voltage must follow. The fundamental idea of this algorithm is to calculate the photovoltaic output power and induce a perturbation.

3.3.2 Squared Output Voltage Regulation

The control law that generates the control signal needs to guarantee that the voltage squared, represented by the equation $y = v_{pv,s}^2$, closely follows a given reference signal, represented by the equation $y^d = v_{pv}^{*2}$. Furthermore, both the signal and its temporal derivative must be available for analysis. Based on these requirements, a first-order filtered PI controller is proposed as a solution:

$$\beta = \frac{b}{b + s}\left(k_p e_4 + k_i e_5\right) \tag{23}$$

where,

$$e_4(t) = y^*(t) - y(t) \tag{24.a}$$

$$e_5(t) = \int_0^t e_4(\tau)\, d\tau \tag{24.b}$$

3.4 Stability properties of the PV-MMC system controlled by ADRC

The system we are examining is characterized by the dynamics in equations (8.a)-(8.d). The dynamic exhibits first-order behavior in response to external and potential internal disturbances. The uncertainties are compensated for by utilizing an ADRC strategy formed in two cascading loops:

- The grid current i_g is stabilized by an inner loop through a filtered PI controller, supplemented by an ESO, which reconstructs the aggregate disturbance online. This disturbance is compensated in the control, reducing the dynamics to a simpler form:

$$\frac{dx_g}{dt} = f_g\left(x_g, t\right) + b_g u(t) \tag{25}$$

By this means, the ESO facilitates dynamic decoupling between disturbances and system behavior [14].

- The slower external loop stabilizes a large magnitude, here v_{pv}, assuming the internal loop responds correctly to setpoints. This uses the temporal separation of dynamics (which one usually can rely upon in cascaded systems).

Under this context, stability can be explained for the overall system by the following properties:

Property 1. *The ESO enables active disturbance compensation, converting the uncertain system into a pseudo-linear one* [12].

Property 2. *The PI controller ensures local stabilization in the inner loop.*

Property 3. *The system has a cascade structure, which is known to ensure semi-global stability under certain conditions* [15], *namely:*

- stability within each sub-loop

- enough separation between dynamic speeds.

Therefore, without a strict Lyapunov analysis, these structural considerations allow us to predict the stability of closed-loop behavior, verified by simulation. This line of argumentation is widely used within robust nonlinear control, especially in the case of electro-energetic systems subject to rapid disturbances.

4 Results & Discussion

The numerical evaluation of the MMC-PV system was carried out in the MATLAB/Simulink environment employing the proposed ADRC control scheme. The results are presented under two operating scenarios: (i) standard climate, with temperature ($T = 25°\text{C}$) and irradiance ($G = 1000\text{W/m}^2$). and (ii) variable climatic conditions to assess the robustness of the proposed controller. In addition, a comparative analysis with conventional control strategies (PI and PR controllers) is performed to highlight the effectiveness and superior performance of the proposed method. The detailed parameters of the power system are summarized in Table 1.

Table 1. Global system parameters: plant and controller

Subsystem	Symbol	Value
Electrical grid	v_g	$220\sqrt{2}$ V / 50 Hz
	r_g, L_g	0.005 mΩ, 2 mH
PV System	C_{pv}	9 mF
DC/AC Converter (MMC)	C_{SM}	1 mF
	r, L	0.05 mΩ, 0.1 mH
Switching frequency	f_e	10 kHz
Number of SM	n	8
ADRC Regulator	ω_c	1.5×10^3
	ω_0	1.1×10^4
PI Regulator	k_p	$1 \times 10^{-3} V^{-2} \Omega^{-1}$
	k_i	$1 \times 10^{-2} V^{-2} \Omega^{-1} s^{-1}$

4.1 Climatic conditions: Standard effect

The simulation results are presented in figures 4 – 8, which demonstrate the efficacy of the proposed ADRC controller under standard climatic conditions. Figure 4. shows that the voltage of the photovoltaic system follows its reference signal. Furthermore, figure 5. illustrates that the active power produced by the photovoltaic system is fed into the network. Figure. 6 and figure 7 demonstrate that the current in the grid and the circulating current align with their respective reference signals, exhibiting a high degree of precision. Finally, figure. 8. demonstrates that the grid current is sinusoidal and in phase with the grid voltage, thus resulting in a unit power factor being achieved.

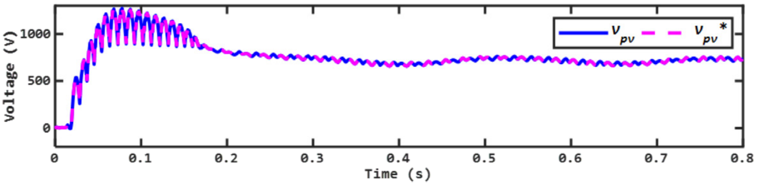

Figure 4. PV voltage along with its corresponding reference.

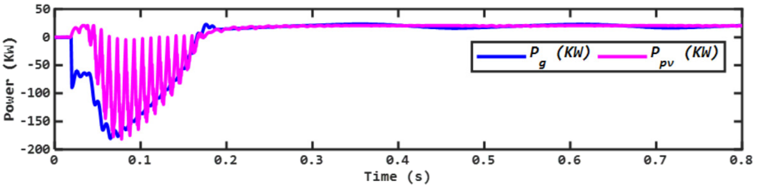

Figure 5. Grid and PV power.

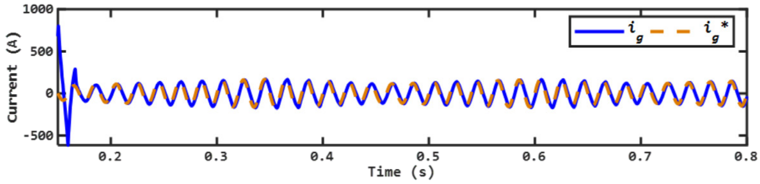

Figure 6. Current of the grid along with its corresponding reference.

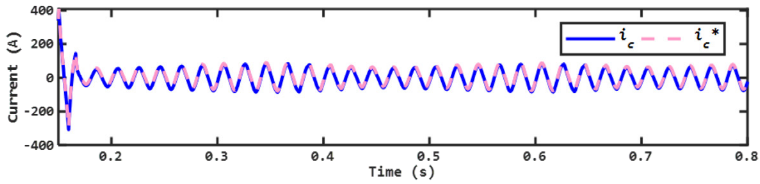

Figure 7. Current in circulation along with its corresponding reference.

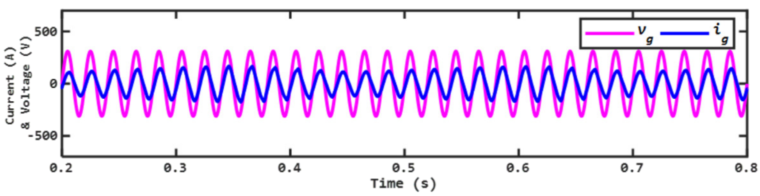

Figure 8. Check the power factor.

4.2 Climatic conditions: Change effect

The controller performance is tested by considering changing irradiation conditions while maintaining a constant temperature of $T = 25\,°\mathrm{C}$. Initially, the irradiance G decreased from $1000\,\mathrm{W/m^2}$ to $700\,\mathrm{W/m^2}$ at $0.4s$ (see figure 9).

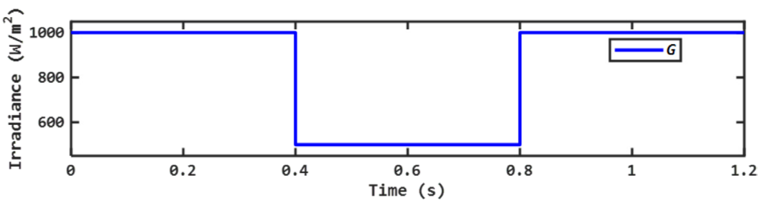

Figure 9. Irradiation pattern.

This change in irradiance resulted in a decrease in power (see figure 10). Figure 11 shows that the PV system voltage follows its reference. Furthermore, the amplitude of the grid and the circulating current increased and remained in phase with the voltage of the network (see figure 12, figure 13, and figure 14). The increase in irradiance from $700\,\mathrm{W/m^2}$ to $1000\,\mathrm{W/m^2}$ at $1s$ results in an increase in output power, and also the grid current decreases, while maintaining a constant power factor.

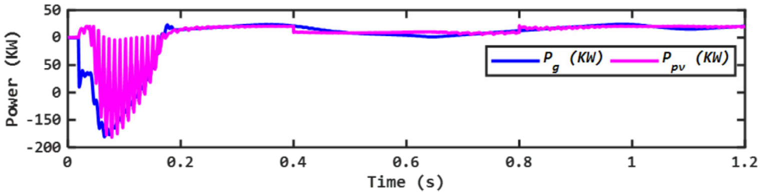

Figure 10. Grid and PV power under irradiance changes.

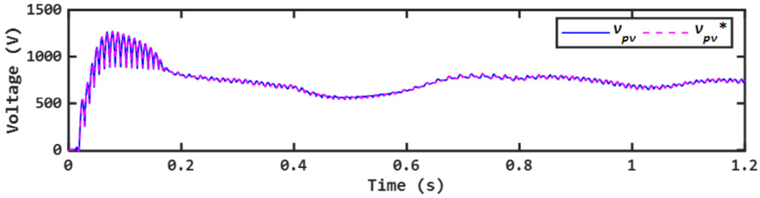

Figure 11. PV voltage along with its corresponding reference under irradiance changes.

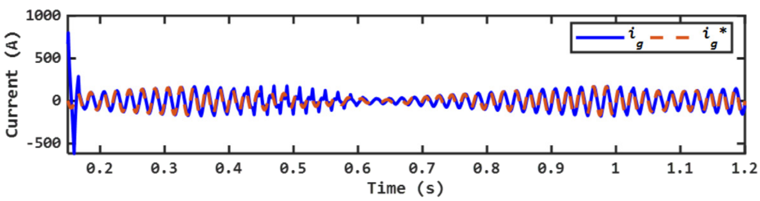

Figure 12. Current of the grid along with its corresponding reference under irradiance changes.

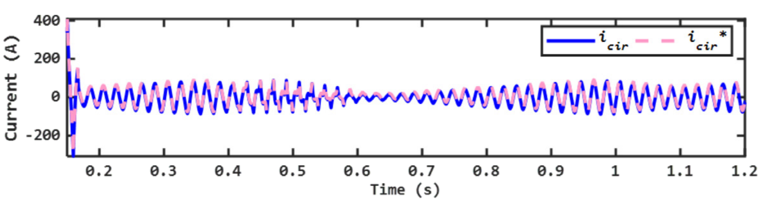

Figure 13. Current in circulation along with its corresponding reference under irradiance changes.

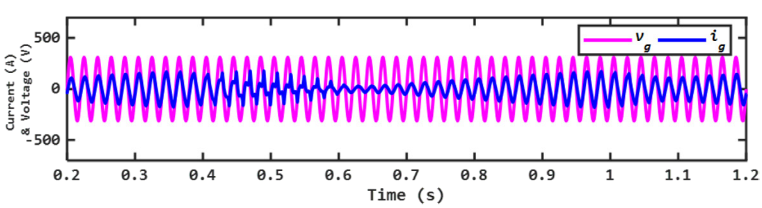

Figure 14. PFC checking under irradiance changes.

4.3 Comparative analysis with literature

To further validate the proposed ADRC-based control strategy's effectiveness, a comparative analysis with recent control approaches reported in the literature is carried out. Table 2 presents a comparative analysis of three control strategies commonly used in Modular Multilevel Converter (MMC) applications, namely the Proportional–Resonant (PR) controller, the adaptive PI controller with fuzzy logic, and the Active Disturbance Rejection Control (ADRC).

Table 2. Comparison of Different Control Strategies for MMC Applications

Criterion	**PR Controller** [8, 9]	**Adaptive PI Controller** [8]	**ADRC**
Operating Principle	Sinusoidal reference tracking using resonant compensation	Dynamic tuning of PI gains through fuzzy logic adaptation	ESO combined with a nonlinear control law
Robustness	Moderate robustness; sensitive to disturbances and parameter variations	Improved robustness due to adaptive fuzzy tuning	Very high robustness with active disturbance and uncertainty rejection
Implementation Complexity	Moderate complexity; requires resonant gain tuning	Moderate complexity; fuzzy rules and membership functions must be designed	Higher complexity due to ESO tuning and observer parameter adjustment
Dynamic Performance	Good steady-state AC tracking, but relatively slow transient response	Fast and stable transient response	Very fast transient response with low overshoot
Impact on MMC Performance	Effective output current regulation	Improved balancing of submodule capacitor voltages	Active suppression of disturbances, circulating currents, and grid imbalances

The comparison highlights key performance criteria, including operating principle, robustness, implementation complexity, dynamic behavior, and overall impact on MMC performance. It can be observed that the PR controller offers satisfactory steady-state tracking of sinusoidal references but exhibits limited robustness and relatively slower transient response under parameter variations and disturbances. The adaptive PI controller improves system performance by dynamically tuning control gains using fuzzy logic, resulting in enhanced robustness and faster transient behavior, although at the cost of increased design complexity. In contrast, the ADRC approach demonstrates superior performance in terms of disturbance rejection, robustness against uncertainties, and transient response speed due to the use of an ESO and active compensation of internal and external disturbances. However, this improved performance comes with higher implementation complexity. Overall, the table emphasizes the trade-off between simplicity, robustness, and dynamic performance among the considered control strategies in MMC applications.

5 Conclusion

This paper presented a grid-connected system's control strategy for single-phase PV–MMC based on the ADRC technique. The proposed cascaded control structure combines an ADRC-based inner loop with a filtered nonlinear PI outer loop to achieve effective regulation of the grid current, circulating current, and PV voltage. In addition, the MPPT P&O algorithm was employed to ensure maximum power extraction under varying atmospheric conditions.

The obtained simulation results demonstrated that the proposed controller provides fast dynamic response, accurate reference tracking, improved disturbance rejection capability, and stable operation under irradiance variations. Moreover, the proposed approach successfully achieves PFC while ensuring efficient transfer of the PV-generated power to the electrical grid. A comparative analysis with conventional PI and PR controllers also confirmed the superior performance of the ADRC-based strategy in terms of robustness, transient response, and disturbance suppression.

The suggested control strategy demonstrates the ADRC's effectiveness for single-phase PV–MMC applications and highlights its potential as a reliable solution for enhancing system stability, robustness, and power quality in grid-connected renewable energy conversion systems.

References

1. O. Arich, A. Abouloifa, A. El Boudali, M.S. Al Numay, A. El Aroudi, A multi-loop nonlinear control approach for a reduced-switch-count grid-tied pv system, Electric Power Systems Research **260**, 113352 (2026). https://doi.org/10.1016/j.epsr.2026.113352
2. J. Zheng, J. Du, B. Wang, J.J. Klemeš, Q. Liao, Y. Liang, A hybrid framework for forecasting power generation of multiple renewable energy sources, Renewable and Sustainable Energy Reviews **172**, 113046 (2023). https://doi.org/10.1016/j.rser.2022.113046
3. O. Arich, A. Abouloifa, I. Lachkar, S. Echalih, M. Aourir, A. El Boudali, N. Hourri, Nonlinear Controller Design for Photovoltaic Powered Single-Inductor Dual-Output Boost DC-DC Converter, in *International Symposium on Automatic Control and Emerging Technologies* (Springer, 2023), pp. 475–484
4. R. Marquardt, Current rectification circuit for voltage source inverters with separate energy stores replaces phase blocks with energy storing capacitors, German Patent (DE10103031A1) **25** (2002).
5. R.H. Chandio, F.A. Chachar, J.B. Soomro, J.A. Ansari, H.M. Munir, H.M. Zawbaa, S. Kamel, Control and protection of mmc-based hvdc systems: A review, Energy Reports **9**, 1571 (2023). https://doi.org/10.1016/j.egyr.2022.12.056
6. M.M. Bhesaniya, A. Shukla, Current source modular multilevel converter: Detailed analysis and statcom application, IEEE Transactions on Power Delivery **31**, 323 (2015). https://doi.org/10.1109/TPWRD.2015.2465152
7. A.G. Abo-Khalil, S.B. Bashir, M.M. Farag, A.A.A. Ismail, A.K. Hamid, N.T. Mbungu, R.C. Bansal, A. Elnady, N. Patel, Direct modulation in mmc-based multiterminal hybrid microgrid: A solution for arm capacitor voltage balancing under unbalanced power distribution, International Journal of Electrical Power & Energy Systems **162**, 110274 (2024). https://doi.org/10.1016/j.ijepes.2024.110274
8. M. Ishfaq, W. Uddin, K. Zeb, I. Khan, S. Ul Islam, M. Adil Khan, H.J. Kim, A new adaptive approach to control circulating and output current of modular multilevel converter, Energies **12**, 1118 (2019). https://doi.org/10.3390/en12061118
9. W. Uddin, K. Zeb, M. Adil Khan, M. Ishfaq, I. Khan, S.u. Islam, H.J. Kim, G.S. Park, C. Lee, Control of output and circulating current of modular multilevel converter using a sliding mode approach, Energies **12**, 4084 (2019). https://doi.org/10.3390/en12214084
10. A. El Boudali, A. Abouloifa, I. Lachkar, M. Aourir, C. Aouadi, O. Arich, N. Hourri, Modeling and Control of Single-Phase Modular Multilevel Converter Using Backstep-

ping Approach, in *International Symposium on Automatic Control and Emerging Technologies* (Springer, 2023), pp. 808–816
11. J. Han, From pid to active disturbance rejection control, IEEE transactions on Industrial Electronics **56**, 900 (2009). https://doi.org/10.1109/TIE.2008.2011621
12. Z. Gao, Scaling and bandwidth-parameterization based controller tuning, in *Proceedings of the 2003 American Control Conference, 2003.* (2003), Vol. 6, pp. 4989–4996
13. D. Li, Z. Wang, W. Yu, Q. Li, Q. Jin, Application of ladrc with stability region for a hydrotreating back-flushing process, Control Engineering Practice **79**, 185 (2018). https://doi.org/10.1016/j.conengprac.2018.07.011
14. J.Q. Han, Auto disturbance rejection controller and it's applications, Control and decision **13**, 19 (1998).
15. H. Khalil, Nonlinear Systems, Pearson Education (Prentice Hall, 2002), ISBN 9780130673893, https://books.google.co.ma/books?id=t_d1QgAACAAJ